

## RESEARCH ARTICLE

10.1002/2013JB010576

## Key Points:

- We perform decompression experiments to simulate the ascent of bubbly magmas
- Void expansion propagates upward by film ruptures to originate outgassing
- Film rupturing causes efficient outgassing and explosive gas emission

## Supporting Information:

- Readme
- Animation S1

## Correspondence to:

A. Namiki,  
namiki@eps.s.u-tokyo.ac.jp

## Citation:

Namiki, A., and T. Kagoshima (2014), Intermittent and efficient outgassing by the upward propagation of film ruptures in a bubbly magma, *J. Geophys. Res. Solid Earth*, 119, 919–935, doi:10.1002/2013JB010576.

Received 31 JUL 2013

Accepted 16 JAN 2014

Accepted article online 21 JAN 2014

Published online 12 FEB 2014

## Intermittent and efficient outgassing by the upward propagation of film ruptures in a bubbly magma

Atsuko Namiki<sup>1</sup> and Takanori Kagoshima<sup>2</sup>

<sup>1</sup>Department of Earth and Planetary Science, University of Tokyo, Tokyo, Japan, <sup>2</sup>Atmosphere and Ocean Research Institute, University of Tokyo, Chiba, Japan

**Abstract** We simulated the ascent of bubbly magma in a volcanic conduit by slow decompression experiments using syrup foam as a magma analogue. During decompression, some large voids appear in the foam. The expansion of one void deep in the foam leads to another void expansion, and the void expansion then propagates upward. The void expansion finally reaches the surface of the foam to originate outgassing. The velocity of the upward propagation of void expansions is essentially the same as the rupturing velocity of the bubble film, suggesting that the rupture of films separating each void propagates upward to create the pathway for outgassing. The calculated apparent permeability of decompressed foam can become higher than that measured for natural pumices/scoriae. The upward propagation of film ruptures thus allows for efficient outgassing. This may also appear as the mechanism for energetic gas emissions originating at a depth, such as Strombolian eruptions.

## 1. Importance of Film Ruptures on Outgassing

It has been widely recognized that outgassing from preruptive magma determines the subsequent volcanic eruption styles [e.g., Eichelberger *et al.*, 1986; Klug and Cashman, 1996; Barmin *et al.*, 2002; Houghton *et al.*, 2004; Shinohara, 2008; Gonnermann and Manga, 2013]. The explosivity of dry eruptions depends on the amount of volcanic gasses within the magma. This is because silicate melt itself does not have enough compressibility to explosively expand, while the gas existing in the magma as bubbles can expand explosively by a rapid decompression [Spieler *et al.*, 2004; Namiki and Manga, 2008; Parfitt and Wilson, 2008]. The interconnected bubbles generated by coalescence may enable permeable gas flow and cause outgassing. When permeable gas flow in bubbly magma is sufficiently fast, the outgassing may preclude explosive eruption [e.g., Mueller *et al.*, 2008; Rust and Cashman, 2011]. However, the idea of permeable outgassing [Eichelberger *et al.*, 1986; Klug and Cashman, 1996] has originated from structures of solid pumice/scoriae, which can maintain the shape of the permeable network. In contrast, in the foam of a molten magma, each bubble is surrounded by melt films; hence, vesicular magma is not necessarily permanently permeable but may transiently become permeable [Namiki and Manga, 2008; Takeuchi *et al.*, 2009]. The magma foam permeability can be transient rather than constant.

Exsolved volcanic gasses make bubbles and are surrounded by melt. In this paper, we call the melt surrounding bubbles as “bubble film.” To separate the volcanic gasses from the magmatic foam, rupturing of the bubble film is required. Deformation of the bubble film causes the film to rupture, resulting in interconnected bubbles [Burgisser and Gardner, 2005; Okumura *et al.*, 2009; Castro *et al.*, 2012; Namiki, 2012; Moitra *et al.*, 2013]. Indeed, in Stromboli, large bubbles are observed, which may be formed by coalescence and contribute to the outgassing [Polacci *et al.*, 2009]. Large bubbles of various sizes become sources of gas emissions from puffing to Strombolian eruptions [Ripepe *et al.*, 2002; Burton *et al.*, 2007; Colo *et al.*, 2010]. Strombolian eruptions are considered as gas emissions originating at depths and ascending as slugs [Vergnolle and Brandeis, 1996; Seyfried and Freundt, 2000; Burton *et al.*, 2007; James *et al.*, 2009; Aiuppa *et al.*, 2010; Bello *et al.*, 2012; Pioli *et al.*, 2012]. However, it still remains unclear how a large-gas slug is generated and how the slug ascends within the bubbly magma.

In contrast, geochemical observation of volcanic gasses shows that substantial outgassing from magmas at shallow depths occurs without eruption [Shinohara, 2008; Edmonds *et al.*, 2009]. Gas saturation pressure, which is correlated with the exsolved depth, can be estimated from the ratio of observed volcanic gas species. Large amounts of gas exsolution at a shallow depth without eruption suggest that the degassed magmas close to the vent are segregated from the volcanic gas and return to the

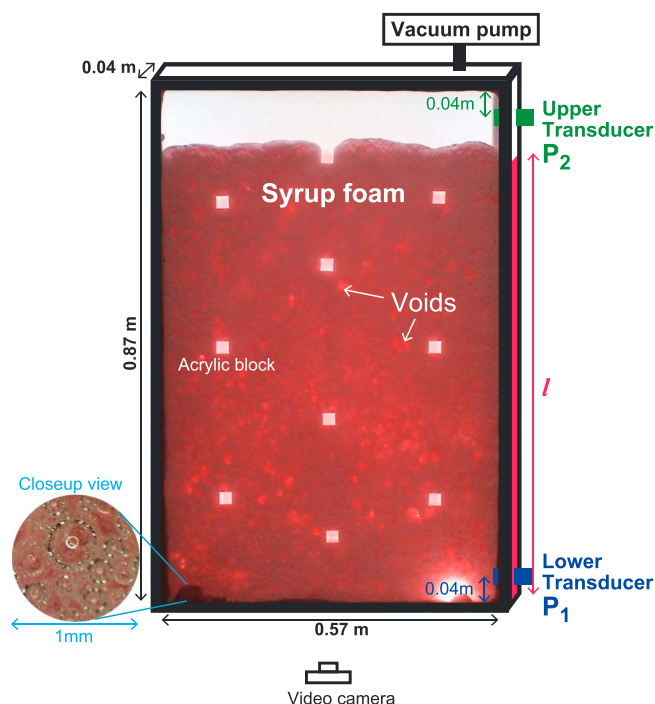


**Figure 1.** Schematic diagram of the apparatus with a still photograph of the experiment of Run 1 at 209 s.

depths without eruption. This mechanism has been recognized as the magma column convection model [Shinohara, 2008; Palma *et al.*, 2011].

Details of a film rupture have been studied in isolated bubbles and droplets [e.g., Debregeas *et al.*, 1998; Kobayashi *et al.*, 2010; Oldenziel *et al.*, 2012; Nguyen *et al.*, 2013]. In a two-dimensional foam, it is observed that the generation and coalescence of large voids by film ruptures dominate the gas separation [Burnett *et al.*, 1995; Hasmy *et al.*, 1999]. Similar phenomena have also been reported for immiscible fluids with a large viscosity contrast [Sato and Sumita, 2007].

Here we examine whether the decompression associated with magma ascent may be able to cause transient outgassing. Decompression leads to the expansion of bubbles, resulting in the thinning of bubble films and making them rupture. Film ruptures may generate interconnected structures of bubbles that segregate the volcanic gas from the surrounding magmatic foam. For this paper, we decompressed syrup foam as a magma analogue to simulate the ascent of bubbly magma in a conduit. The syrup has a viscosity and surface tension similar to those of basaltic magma so we can apply our experimental results directly to the real magma system. Experiments show that the upward propagation of film ruptures creates a pathway for energetic gas emissions.

## 2. Experimental Methods

We conducted slow decompression experiments in an acrylic tank with inner dimensions of 0.57 m (width), 0.87 m (height), and 0.04 m (depth) as shown in Figure 1. To prevent the walls from warping during decompression, 10 acrylic blocks were placed in the tank. For our magma analogue, we used syrup solutions. Experimental conditions are summarized in Table 1, and notations are summarized in Table 2. By varying the water content of the syrup, we changed its viscosity between 12 and 4300 Pa s, which covers the typical viscosity range of basaltic melts, between 10 and  $10^3$  Pa s [e.g., Giordano and Dingwell, 2003], and most preerupted andesitic melts,  $< 10^4$  Pa s [e.g., Takeuchi, 2011]. The density of the syrup itself is between 1400 and 1452 kg m<sup>-3</sup>, which is smaller and of the same order of magnitude as that for the typical density of basaltic melt, approximately 2700 kg m<sup>-3</sup>. We infer that this small difference in the density between the real magma and our syrup does not prevent us from applying our experimental results to real volcanic outgassing. The density difference between the liquid and gas phases is important for bubble ascent and

**Table 1.** Experimental Conditions and Results<sup>a</sup>

		Run 1 Red Cross	Run 2 Pink, Red Asterisk	Run 3 Light Blue Diamond	Run 4 Green Square	Run 5 Green Circle	Run 6 Blue Triangle	Run 7 Blue Plus Sign
Viscosity $\eta$	Pa s	12	12	220	920	920	4300	4300
Initial $\phi$	–	0.81	0.73	0.20	0.72	0.74	0.68	0.54
Final $\phi$	–	0.93	0.91	0.88	0.85	0.87	0.92	0.61
Mean $\phi$	–	0.91	0.84	0.82	0.80	0.84	0.90	0.60
$\phi$ to begin outgassing	–	0.87	0.88	–	0.72	0.82	0.68	0.54
Min $P_1$	Pa	$12 \times 10^3$	$11 \times 10^3$	$11 \times 10^3$	$23 \times 10^3$	$27 \times 10^3$	$9 \times 10^3$	$4 \times 10^3$
Max $-dP_1/dt$	Pa/s	$4 \times 10^3$	$1 \times 10^3$	$6 \times 10^3$	$1 \times 10^3$	$4 \times 10^3$	$6 \times 10^3$	$6 \times 10^3$
Max $k$	m <sup>2</sup>	$2 \times 10^{-10}$	$3 \times 10^{-11}$	–	$2 \times 10^{-11}$	–	$1 \times 10^{-11}$	$1 \times 10^{-10}$
Initial $D$	mm	0.19	0.27	0.10	0.26	0.28	0.39	0.49
Void size at Max $k$	m	0.01	0.01	–	0.01	–	0.04	–
$V_s$	m <sup>3</sup>	$1.4 \times 10^{-3}$	$0.8 \times 10^{-3}$	$2.0 \times 10^{-3}$	$1.3 \times 10^{-3}$	$0.5 \times 10^{-3}$	$1.5 \times 10^{-3}$	$2.3 \times 10^{-3}$
Characteristic Propagation		Observed	Observed	Observed	Observed	Small $V_s$	Observed	Wait

<sup>a</sup>Viscosity is for bubble-free syrup,  $\phi$  is the volume fraction of gas, the minimum  $P_1$  is the measured minimum pressure inside the foam, the maximum  $-dP_1/dt$  is the averaged decompression rate for the first 10 s,  $k$  is the apparent permeability calculated from equation (6). In Run 3 (light blue), chemical reaction increases the gas fraction inside foam during the decompression so that occurrence of outgassing cannot be evaluated. For Run 5, the pressure difference between two transducer is too low to calculate  $k$ .  $D$  is the bubble diameter. We measured the typical bubble diameter from the close-up view as shown in Figure 1 before we began the decompression. Large voids appear during the decompression, as shown in Figure 1. Details of the characteristics are described in the experimental methods section. The propagation of void expansion is shown in Figure 2. Colors and symbols correspond to those in Figures 3a and 6.

compaction; neither phenomenon is significant in our experiments. Bubbles are created through a chemical reaction between baking soda and citric acid, generating carbon dioxide. Using this method, a foam with a bubble fraction of  $\phi > 0.5$  is easily made.

We estimate that the surface tension between the syrup and carbon dioxide is similar to that between the silicate melt and volcanic gasses. This is because the surface tension between the aqueous sugar solution and air is similar to that of pure water,  $0.07 \text{ N m}^{-1}$  [e.g., Lindfors, 1924]. The surface tension between the

**Table 2.** Notation

Parameter	Unit	Description
$k$	m <sup>2</sup>	Apparent permeability
$l$	m	Average height of the foam
$R$	m	Void radius
$V_{fm}$	m <sup>3</sup>	Foam volume measured by visual observation
$V_s$	m <sup>3</sup>	Syrup volume in foam
$V_{gm}$	m <sup>3</sup>	Gas volume inside the foam calculated from $V_{fm} - V_s$
$V_i$	m <sup>3</sup>	Time-dependent gas volume initially located inside the foam
$v_r$	m s <sup>-1</sup>	Rupturing velocity of bubble film
$v_p$	m s <sup>-1</sup>	Propagation velocity of void expansion
$v_{or}$	m s <sup>-1</sup>	Outgassing velocity
$v_{or}/l$	s <sup>-1</sup>	Outgassing rate
$P_1$	Pa	Pressure measured by the transducer inside the foam
$P_2$	Pa	Pressure measured by the transducer above the foam
$P_a$	Pa	Atmospheric pressure
$p$	Pa	Overpressure inside bubble
$p_0$	Pa	Initial overpressure inside bubble
$\tau$	s	Timescale until over pressure reduces
$S$	m <sup>2</sup>	Cross section of foam
$t$	s	Time
$r$	m	Aperture radius
$r_0$	m	Initial aperture radius
$r_f$	m	Aperture radius at $t = \tau$
$D$	m	Bubble diameter
$\eta$	Pa s	Viscosity of bubble-free syrup
$\eta_g$	Pa s	Viscosity of gas
$\rho$	kg m <sup>-3</sup>	Density of bubble-free syrup or magma
$\rho_g$	kg m <sup>-3</sup>	Density of gas
$\phi$	–	Volume fraction of gas inside the foam calculated from $V_{gm}/V_{fm}$
$e$	m	Film thickness
$\gamma$	N m <sup>-1</sup>	Surface tension
$C_g$	m s <sup>-1</sup>	Sound velocity

silicate melt and water is on the order of a magnitude of  $0.1 \text{ N m}^{-1}$  [e.g., *Bagdassarov et al.*, 2000; *Mangan and Sisson*, 2005; *Gardner*, 2012]. The syrup foam is dyed a reddish color for visualization. Given that the syrup foam is opaque, we illuminated the tank by a surface backlighting source to visualize the distribution of large voids made by the expansion and coalescence of small bubbles. Although our tank is quasi two dimensional, its depth of 0.04 m is greater than the size of most of the largest void (0.01 m). Thus, we consider that our experiments are applicable to both two-dimensional dikes and three-dimensional (cylindrical) conduits. These are the same techniques that we used in *Namiki and Manga* [2008] and *Namiki* [2012]. We do not consider the effect of phenocrysts. Decompression experiments of crystal (corundum)-bearing rhyolite have shown that preexisting crystals do not affect the bubble size distribution and bubble connectivity [*Okumura et al.*, 2012].

We introduced syrup foam inside the tank and then decompressed it using a vacuum pump. We measured the pressure inside and outside the foam using pressure transducers located at the top and bottom of the tank with a sampling rate of 5 Hz. The nominal accuracy and repeatability of transducers for all measurable ranges are  $<1250 \text{ Pa}$  and  $<250 \text{ Pa}$  for the lower transducer and  $<5000 \text{ Pa}$  and  $<1000 \text{ Pa}$  for the upper transducer, respectively. Within the pressure ranges in our experiments, we estimate the accuracy and repeatability for both transducers are  $<500 \text{ Pa}$  and  $<100 \text{ Pa}$ , respectively, and verify that in decompressing an empty vessel, the difference in the measured values between the two transducers is within  $<250 \text{ Pa}$ . Thus, we consider the resolution of pressure is  $<1000 \text{ Pa}$  for the absolute value and  $<250 \text{ Pa}$  for the relative difference. All of experiments were conducted at pressures higher than  $>1000 \text{ Pa}$  (Table 1). We used the measured pressure difference between two transducers to obtain apparent permeabilities. Maximum permeabilities in Table 1 are calculated when the pressure differences are  $>1000 \text{ Pa}$ .

We calculate the maximum decompression rate  $-dP_1/dt$  in Table 1 by averaging the pressure change measured by the lower sensor  $P_1$  for the initial 10 s. If the ascending magma velocity is related to the decompression rate by  $\rho g v \sim dP/dt$ , the maximum decompression rates in our experiments  $-dP_1/dt \sim 10^3 \text{ Pa s}^{-1}$  are equivalent to the ascending velocity of  $10^{-1} \text{ m s}^{-1}$ , where  $\rho \sim 10^3$  is the density of bubbly magma and  $g = 9.8 \text{ m s}^{-2}$  is the gravitational acceleration. The decompression rate becomes lower as time elapses, and the pressure inside the tank eventually approaches the minimum value. We vary the decompression rate and minimum pressure by leakage.

The sequence of foam expansion is recorded with a high-resolution video camera that takes 30 frames per second with a resolution of  $1440 \times 1080$  pixels. We calculate the volume change of the decompressed foam as the product of the two-dimensional foam image and the fixed tank depth of 0.04 m. In reality, the depth of the foam is thinner than 0.04 m at the top of the foam because of its mounded shape, but we use the ridgelines to calculate the two-dimensional images. Consequently, the calculated foam volume becomes a maximum estimate so that the calculated outgassing volume and the permeability become minimum estimates. When we calculate the foam volume, we exclude the volume of the acrylic blocks. Except for Run 3, we began the decompression after the volume increase of the foam by chemical reaction decelerates. The chemical reaction inside the foam may still continue during the experiments, which increases the real outgassing volume but is not included in our estimate. The measured maximum expansion rate by chemical reaction is less than 10% of that expected by decompression. When calculating the initial foam volume, we do not consider the syrup that adheres to the tank wall; this results in an increase of the error to 10% but does not affect the experimental results significantly. The experiments were begun at atmospheric pressure (1004–1019 hPa) and were conducted at room temperature (17–22°C), so that water evaporation from the syrup during decompression was negligible.

We performed seven experiments with four different viscosities, as summarized in Table 1. In Run 2, we decompressed the syrup foam twice; i.e., we decompressed it to  $8.5 \times 10^4 \text{ Pa}$ , compressed it to atmospheric pressure, and then decompressed it again to  $1.1 \times 10^4 \text{ Pa}$ . In this experiment, we also changed the decompression rate intermittently. In Run 3, we decompressed the foam before the chemical reaction creating bubbles ended so that both the initial bubble size and bubble fraction in the foam became small. As a result, the gas mass inside the foam increases at least 3 times during the decompression. We thus do not discuss the occurrence of outgassing for this experiment. In Run 5, the syrup volume was less than in the other experiments. In Run 7, we waited 1 day after making the foam to start the experiment so that the bubble size in the foam became larger than in the other experiments.

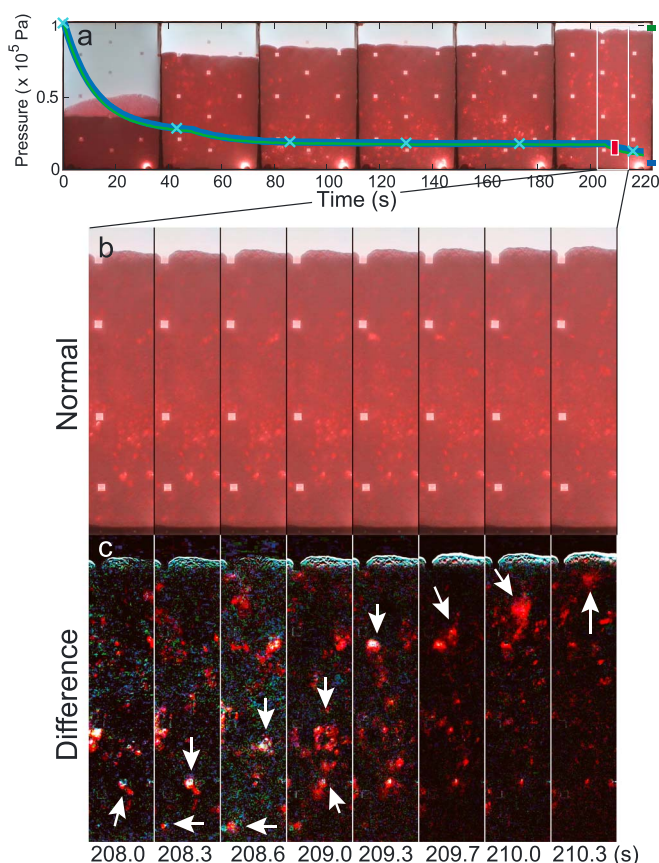


**Figure 2.** (a) Overview of the experiment of Run 1. As the pressure inside the tank becomes lower, the syrup foam expands. The blue and green curves show the time variation of pressure measured at the bottom and top of the tank, respectively, as denoted by blue and green squares in Figure 1. The light blue cross shows the timing of each photograph. Red and white rectangles show the timing and the region shown in the (b) local photographs of the foam and the (c) differences between the pictures shown in Figure 2b and those taken 0.5 s later. The bright region indicates the occurrence of time variations, such as void expansion. White arrows indicate the propagation of the region where voids are expanding. The numbers indicate the elapsed time after decompression begins.

### 3. Upward Propagation of Film Ruptures

#### 3.1. Experimental Observations

Figure 2a shows an overview of the experiment of Run 1. When the inside of the tank was decompressed, as denoted by Figure 2a (blue and green curves), the syrup foam expanded. As the foam expanded, several large bubbles appeared, as shown in Figure 1. Larger bubbles, generated by the expansion and coalescence of small bubbles, have different behaviors from small bubbles. In order to distinguish large bubbles, we call large bubble void in the following text.

During the expansion of the foam, the expansion of voids propagates upward, as shown in Figure 2c. We find that when a void near the bottom expands (Figure 2c, 208.3 s, upper arrow), the void above it subsequently expands (Figure 2c, 208.6 s, upper arrow), while the lower one shrinks. At 209.0 s, the two voids coalesce into a large void. At 210.0 s, a void close to the surface expands and opens the outlet releasing the gas inside the void to the outside of the foam. Outgassing, thus, occurs. This behavior suggests that the gas trapped inside voids travels upward. Details of the void expansion and its upward propagation are recognizable in animated images (Animation S1 in the supporting information) and by the time difference of still photographs (Figure 2c). Especially, the propagation direction is accurately verified in Animation S1. It is, however, difficult to identify the propagation of void expansion from still photographs (Figure 2b).

We observed similar characteristics in the five experiments listed in Table 1. Note that similar phenomena are observed in Run 3, in which chemical reaction generates carbon dioxide during the decompression. In Run 5, we found large voids in the foam and intermittent movement of the surface associated with outgassing but did not observe the propagation of void expansion. This is because as foam is opaque, some

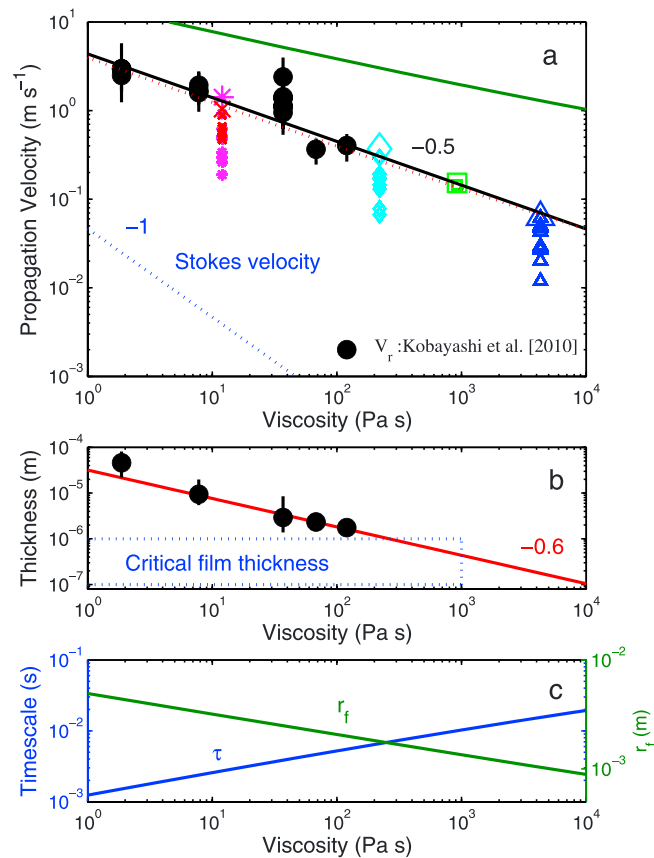


**Figure 3.** (a) Measured propagation velocities of void expansions. Symbols correspond to those listed in Table 1. Large symbols indicate the maximum velocities measured within each experiment. The slope shown by a black line is calculated for the large symbols. Black bullets indicate the measured rupture velocities of bubble film surrounding an isolated bubble [Kobayashi et al., 2010]. Details are provided in Appendix A1. The dotted red line is the film rupture velocity calculated by  $r_f / \tau$  as shown in Figure 3c. The green line indicates the hypothetical rupture propagation velocity of the gas exchange between two coalescing bubbles and is calculated by  $R / \tau$ . The dotted blue line shows the Stokes velocity and is estimated using equation (1). (b) Black bullets indicate the estimated film thicknesses surrounding isolated bubbles using equation (A1). The red line is a fitting line of four black bullets  $\eta > 5$  Pa s. Details are provided in Appendix A2. The blue-dotted rectangle indicates the critical thickness of rupturing film as compiled by Nguyen et al. [2013]. (c) The left-hand y axis and blue line indicate the timescale  $\tau$  until the overpressure inside the bubble reduces in association with a film rupture as calculated by equation (4). The right-hand y axis and green line indicate the aperture radius for  $t = \tau$  calculated by equation (A1).

void expansions may be hidden from view. In Run 5, the height of the foam was small. The propagation distance of void expansions may be too short to be observed. In Run 7, the volume fraction of gas was lower than in other experiments; we do not observe voids in the foam. We infer that the visibility inside the foam depends on the volume fraction of gas. Even when voids exist in the foam with low gas fractions, they are not observed.

Figure 3a summarizes the measured propagation velocities of void expansion. We measured the propagation velocity by observing animations in slow motion. We measured the loci of voids and time at the beginning and end of void propagation and then calculated the propagating velocity, assuming that void expansion propagates in a linear path. When the propagation direction changed halfway through the propagation, we approximated them by polygonal lines. We calculated the average velocity and did not account for time-dependent velocity changes. We repeatedly measured the propagation velocity for the same event and confirmed that the measurement errors associated with this method are within the size of the large symbols. We measured 10 different events in each experiment except for Run 4, in which the final volume of foam is small, and so we found only two events.

Figure 3a shows that the maximum propagation velocity is dependent on viscosity and that the measured propagation velocity varies within the same experiment. This may be because the propagation of void expansion sometimes gets held back at a particular void until the void expands sufficiently.

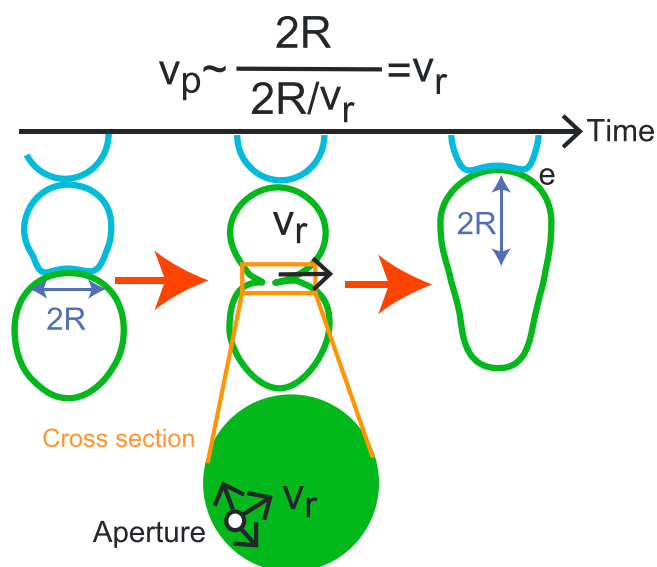


Figure 4. A schematic illustration for the propagation of void expansion and a film rupture.

### 3.2. A Model

#### 3.2.1. Conceptual Model

Our experiments show that the expansion of voids begins deep in the foam and propagates upward. The propagation finally reaches the surface of the foam and causes outgassing. We interpret these results as meaning that the upward propagation of film rupturing occurs as shown in Figure 4 and is observed as the propagation of void expansion. We discuss the details of our hypothesis below.

Figure 4 explains our conceptual model of the propagation of void expansion. When a film between two vertically contacting voids ruptures, the coalescing two voids make one large void. The newly created large void deforms the surrounding film so that another film ruptures. In general, bubble films become thinner in shallower parts of the foam as a result of gravitational drainage, so that the upper films rupture more easily than the lower ones. Void expansion, thus, propagates upward.

If the films separating voids are thin enough to rupture immediately, the propagation velocity is regulated by the rupturing velocity of the film  $v_r$ . The sequence of a film rupture is as follows: first, an aperture appears on the film, and then the aperture grows so that the film disappears (Figure 4, cross section). We call the growth rate of the aperture on the film “the rupturing velocity.” The timescale for removing the film by rupturing is approximately  $2R/v_r$ . When a film ruptures, the void expansion propagates at a length scale of  $2R$ . Accordingly, the propagation velocity coincides with the rupturing velocity,  $v_p = 2R/(2R/v_r) = v_r$ .

To test this hypothesis, we plotted the measured film rupture velocity on an isolated bubble [Kobayashi *et al.*, 2010] in Figure 3a (black bullets). Details of how the black bullets were calculated are given in Appendix A1. Both the maximum propagation velocities and the film rupture velocities are located on the black line with a slope of  $-0.5$ . We interpret Figure 3a as showing that the rupturing velocity regulates the maximum propagation velocity of void expansion. However, when the film is thicker than that critical for rupturing, each void must expand to initiate the rupturing of the film. In this case, the propagation velocity is regulated by the summation of the times for expansion and the film rupture, which explains why the measured propagation velocities for each experiment extend beneath the black line. The scattering of the measured velocity beneath the black line suggests variation in the film thickness.

The blue dotted line in Figure 3a shows the possible ascent velocity of voids by buoyancy estimated using the Stokes velocity

$$v_{st} = \frac{\Delta \rho g R^2}{3\eta}, \tag{1}$$

where we assume typical values for the experiment  $\Delta \rho = (1 - \phi)\rho \sim 140 \text{ kg m}^{-3}$  is the density difference between the foam and gas,  $\phi = 0.9$  is the volume fraction of gas in the foam,  $\rho$  is the density of the

bubble-free liquid, and  $R = 10$  mm is the void radius. The measured propagation velocities of voids are much faster than the Stokes velocity, indicating that the buoyancy-driven bubble ascent cannot explain the upward propagation of void expansion. Note that, in equation (1), we used the viscosity  $\eta$  of bubble-free syrup instead of the viscosity of foam. The viscosity of foam may differ from that of a bubble-free liquid, but it is difficult to measure.

### 3.2.2. Slope of $-0.5$

Next, we consider the origin of the slope of  $-0.5$  observed in Figure 3a and the effect of the gas exchange between two coalescing voids on the propagation velocity.

The rupturing velocity of the film is estimated in two ways. When the inertia effect dominates, the rupturing velocity is controlled by the balance between the capillary and inertial forces [Culick, 1960]

$$v_r = \sqrt{\frac{2\gamma}{e\rho}}, \quad (2)$$

where  $\gamma$  is the surface tension and  $e$  is the film thickness. When the viscous effect dominates, the rupturing velocity is determined by the balance between viscous dissipation and the loss of surface energy [Debregeas et al., 1998]:

$$v_r = \frac{\gamma r}{\eta e}, \quad (3)$$

where  $r$  is the aperture radius.

Using two dimensionless parameters, we infer that the viscous effect dominates the film rupture in our experiments: i.e.,  $Re = \rho v_r e / \eta \ll 1$  and  $Oh = \eta / \sqrt{\rho \gamma R} \gg 1$  [Brenner and Gueyffier, 1999]. The former equation defines the Reynolds number which compares inertia and viscous forces. The latter equation defines the Ohnesorge number, which compares viscous forces to inertia and capillary forces [e.g., McKinley and Renardy, 2011]. Even when rupturing occurs in a viscous regime, the rupturing velocity accelerates following equation (3) until it reaches a maximum estimated by equation (2).

In Figure 3a, the maximum propagation velocity is shown to depend on the viscosity with a slope of  $-0.5$ . Neither rupturing velocities, equation (2) nor equation (3), show dependence on  $\eta^{-0.5}$ . We infer that the viscosity dependence  $v_r \propto \eta^{-0.5}$  appears because film thickness depends on viscosity. Indeed, experimentally estimated film thickness depends on liquid viscosity,  $e \propto \eta^{-0.62}$ , as shown in Figure 3b and discussed in Appendix A2.

Next, we consider the timescale to theoretically calculate film rupture velocity using  $e \propto \eta^{-0.62}$  to compare with experimental results. This is because, substituting equation (A1) into equation (3), we obtain  $v_r = \gamma r_0 / (\eta e) \cdot \exp\{\gamma t / (\eta e)\}$ , which is time (aperture radius) dependent. In Kobayashi et al. [2010], stopping of the aperture growth and the subsequent deflation of the bubble film are observed, suggesting that when pressure inside the bubble is reduced by releasing gas from the aperture, the bubble film loses tensional force, and then the aperture growth stops. Accordingly, we estimated the timescale required for the release of gas from a growing aperture and calculated the averaged rupture velocity within this timescale.

The reduction of overpressure by gas flow within the bubble during the film rupture is written as [Kobayashi et al., 2010]:

$$p = p_0 \exp \left[ \frac{P_a r_0^2}{\rho_g c_g (4/3) R^3} \frac{\eta e}{2\gamma} \left\{ 1 - \exp \left( \frac{2\gamma}{\eta e} \tau \right) \right\} \right], \quad (4)$$

where  $P_a / \rho_g = 10^5 / 1.2$  (Pa/(kg m<sup>-3</sup>)) is a ratio between the surrounding pressure and the gas density,  $c_g = 343$  m s<sup>-1</sup> is the sound velocity of air at 20 °C, and  $r_0$  is the initial aperture radius on a rupturing film.

From equation (4), we calculated the timescale  $\tau$  until the overpressure inside the void was reduced to  $p/p_0 = \exp(-1)$  using experimentally obtained  $e$  and  $r_0$  as written in Appendix A2, and we plotted it with a blue line in Figure 3c. Substituting the timescale  $\tau$  into equation (A1), we obtained the final radius of the aperture  $r_f$  and plotted it in Figure 3c (green line). The ratio of  $r_f/\tau$  becomes an averaged film rupture velocity.

We plotted  $r_f/\tau$  in Figure 3a (red dotted line), which explains the slope of the black line for the propagation velocity. Again, we interpreted Figure 3a as showing that the rupturing velocity regulates the maximum propagation velocity of void expansion.

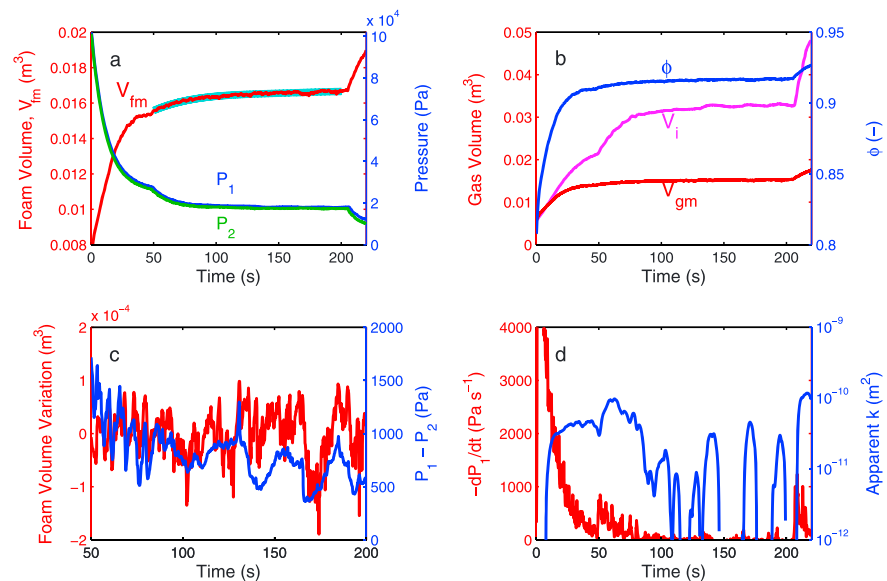


**Figure 5.** Details of outgassing observed in the experiment of Run 1. (a) Foam expansion following decompression. The red curve shows the time-dependent foam volume as measured by visual observation  $V_{fm}$ . The blue and green curves, respectively, show the pressure change inside and outside the foam, as measured by the bottom and top pressure transducers shown in Figure 1. The light blue curve is the fourth-order polynomial approximation of the red curve. (b) The red curve is the gas volume inside the observed foam  $V_{gm} = V_{fm} - V_s$ . The pink curve is the volume change of the gas initially located inside the foam,  $V_i$  and is calculated using equation (5). The difference between curves  $V_i$  and  $V_{gm}$  becomes the accumulated outgassed volume. The blue curve is the calculated volume fraction of the gas inside the foam,  $\phi = V_{gm}/V_{fm}$ . (c) The red curve shows the enhanced fluctuation of the measured foam volume,  $V_{fm}$ , calculated from the difference between the red and light blue curves in Figure 5a. The blue curve shows the difference in pressure inside and outside the foam calculated from  $P_1 - P_2$  in Figure 5a. (d) The red curve shows the decompression rate calculated using  $P_1$ . The blue curve shows the apparent permeability as calculated using equation (6). In Figures 5a–5d, the colors of the curves correspond to those of their reference axes.

### 3.2.3. Gas Exchange

When two vertically contacting voids coalesce, the upper void may be pressurized. This is because the pressure inside the lower void is higher than that of upper one, assuming the foam pressure is static. The pressurized upper void can expand to rupture the surrounding film. This pressurization is another possible mechanism for propagating film ruptures.

However, we consider that the pressurization is not a relevant mechanism in our experiment. This is because the pressure difference between two coalescing voids is estimated to be several tens of pascals from the measured pressure gradient in the foam. This pressure perturbation is approximately 1% of the background pressure and is not enough to deform voids significantly.

In addition, the release of gas to the upper void is faster than the measured propagation velocity. The timescale for pressure change with the release of gas is represented by Figure 3c (blue line). If this pressure change ruptures the next film, that velocity is calculated by  $R/\tau$  and is plotted in Figure 3a (green line), which is much faster than the measured black line.

Thus, we conclude that the pressure changes within voids associated with coalescing occur immediately; then the coalescing voids change their shapes at a rupture velocity, and then the film rupture propagates upward.

## 4. Outgassing

### 4.1. Experimentally Measured Outgassed Volume

Visual observations showed the propagation of film ruptures, which can induce outgassing. In this section, we quantitatively estimate the outgassed volume.

The details of time-dependent outgassing are shown in Figure 5. We measured the time-dependent foam volume  $V_{fm}$  from visual observations (Figure 5a, red curve). Foam expansion correlates with pressure change, as denoted in Figure 5a (blue, green, and red curves). From the observed foam volume  $V_{fm}$  and the constant

volume of syrup  $V_s$ , we obtained the gas volume inside the foam  $V_{gm} = V_{fm} - V_s$ , as denoted by the red curve in Figure 5b. The time-dependent volumetric gas fraction in the foam was calculated by  $\phi = V_{gm}/V_{fm}$  and is denoted by Figure 5b (blue curve).

The volume change of the gas initially confined within the foam,  $V_i$ , is calculated and denoted in Figure 5b (pink curve) and given by

$$V_i = V_{i0} \frac{P_a}{P_1}, \quad (5)$$

where  $V_{i0}$  is the volume of gas confined in the foam at atmospheric pressure  $P_a$ . Equation (5) assumes that the foam expands under isothermal conditions, which explains the volume change of slowly expanding foam without outgassing [Namiki and Manga, 2006].

Given that syrup at room temperature does not evaporate, the difference between the pink and red curves in Figure 5b ( $V_i - V_{gm}$ ) indicates the accumulated outgassed volume at a given pressure. This is a minimum estimate of outgassed volume for the following reasons. (1) As we mentioned in the experimental methods section, we use a two-dimensional image of the foam to calculate the foam volume, assuming that the depth of the foam is equal to that of the tank. In reality, the foam depth is less than that of the tank at the top of the foam, so that the measured outgassed volume becomes a maximum estimate. (2) We neglected the effect of the chemical reaction inside the foam, which supplies newly generated gas inside the foam. (3) We used the pressure  $P_1$  at the bottom of the foam to calculate  $V_i$ . The pressure in the foam close to the surface must be lower than  $P_1$ . The actual volume outgassed through the surface of the foam at the given pressure is larger than the calculated value  $V_i - V_{gm}$  in Figure 5b. Thus, outgassing is confirmed in a quantitative analysis, as well as by visual observation (Figure 2).

In Table 1, we have listed the volumetric gas fraction,  $\phi$ , when outgassing begins. The critical  $\phi$  initiating outgassing shows clear viscosity dependence; i.e., a foam with a viscous liquid begins outgassing at a lower  $\phi$ .

Outgassing occurs intermittently from the large interconnecting voids, which can be observed in the fluctuations of the foam volume,  $V_{fm}$ . Figure 5c (red curve) shows the short-term fluctuation of the foam volume, subtracting the fourth-order polynomial approximation, shown in Figure 5a (thick light blue curve), from Figure 5a (red curve). The fluctuation of the foam volume correlates with the pressure difference inside and outside of the foam,  $P_1 - P_2$ , as shown by Figure 5c (blue curve). Initially, at 50–90 s, high-frequency components of approximately 0.1 Hz are dominant in both, while low-frequency components of approximately 0.04 Hz appear later at 150–200 s. The correlation between the foam volume and the pressure difference indicates that vents for outgassing appear intermittently at the top of the foam. When there are no vents, the foam expands; however, part of the expansion is hindered by viscosity, so the pressure inside the foam increases. Once a vent opens, outgassing occurs, which decreases both the foam volume and the pressure inside the foam. The low-frequency components in Figure 5c indicate that the occurrence of outgassing becomes infrequent as time elapses at a slow decompression rate.

Although outgassing in our experiments occurred intermittently, calculating the apparent permeability is helpful for comparing our results with the previously measured permeability for natural samples. We can calculate the apparent permeability,  $k$ , assuming Darcy's law,

$$v_{or} = \frac{k}{\eta_g} \frac{P_1 - P_2}{V_{fm}/S}, \quad (6)$$

where  $\eta_g = 1.8 \times 10^{-5}$  Pa s is the viscosity of air and  $S$  is the cross section of the foam. Here we assumed that the pressure outside the foam is a uniform  $P_2$  so that the pressure gradient becomes  $dP/dl = (P_1 - P_2)/(V_{fm}/S)$ . We calculated the outgassing velocity  $v_{or}$  by

$$v_{or} = \frac{1}{S} \left( -\frac{V_{gm}}{P_1} \frac{dP_1}{dt} - \frac{dV_{gm}}{dt} \right). \quad (7)$$

On the right-hand side of equation (7), the first term indicates the possible change in the volume of gas inside the foam associated with decompression under constant temperature; the second term shows the measured change in the volume of gas inside the foam. The difference between these two terms becomes

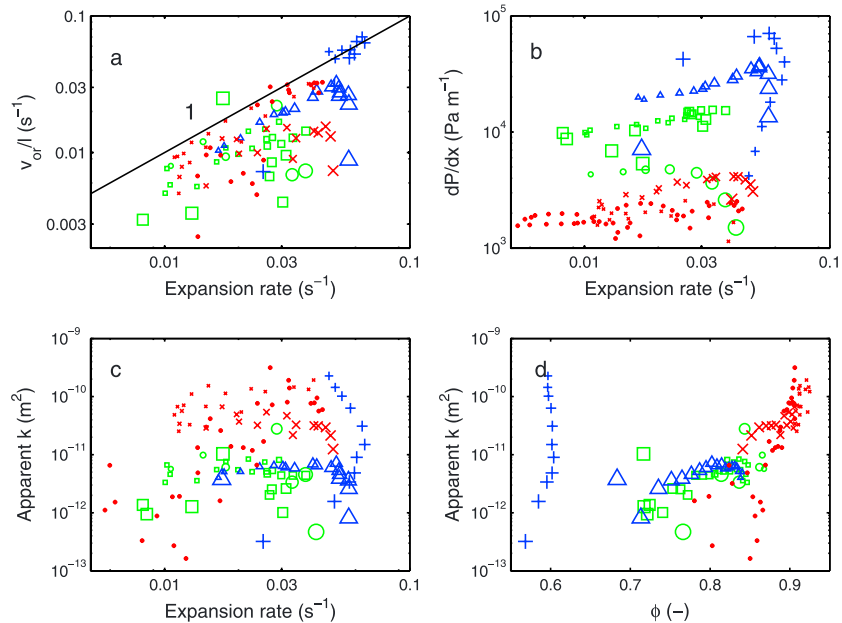


**Figure 6.** Summary of the characteristics of outgassing. (a) Each sequence of symbols indicates the time evolution of the outgassing rate,  $v_{or}/l$ , defined by equation (9) as a function of the expansion rate, equation (8). Different symbols indicate the different experiments (Table 1). Symbols become smaller as time elapsed. Colors of symbols indicate viscosity: red, green, and blue are 10, 920, and 4300 Pa s, respectively. In the experiment denoted by plus sign, the bubble size in the foam is larger than that in other experiments. (b) Time evolution of the vertical pressure gradient within the foam as calculated by  $(P_1 - P_2)/(V_m/S)$  as a function of the expansion rate. (c) Time evolution of apparent permeability as defined by equation (6) as a function of the expansion rate. (d) Time evolution of apparent permeability as a function of the gas volume fraction in the foam. In Figures 6a–6d, we plotted the average values for 2 s when both the vertical pressure difference and the decompression rate were sufficiently large,  $P_1 - P_2 > 250$  Pa and  $dp/dt > 250$  Pa s<sup>-1</sup>, respectively.

the outgassed volume. In the actual data, both the pressure gradient and the outgassing velocity have short-time temporal variations. Thus, we used a low-pass filter of 20 s for  $dP/dl$  and  $v_{or}$  to calculate the apparent permeability.

We did not account for the effect of inertia on permeability [Rust and Cashman, 2004] because the estimated Reynolds number is  $Re \leq 1$ , where  $Re = \rho_g v_{or} R / \eta_g$ . Here,  $\rho_g \sim 10^{-1}$  kg m<sup>-3</sup> is the gas density at 10<sup>4</sup> Pa,  $v_{or} \sim 10^{-2}$  m s<sup>-1</sup> is the outgassing velocity,  $R < 10^{-2}$  m is the void radius, and  $\eta_g \sim 10^{-5}$  Pa s is the gas viscosity.

Figure 5d (blue curve) shows the apparent permeability calculated by equation (6) as a function of time. The peaks of the envelopes in the calculated values are roughly  $10^{-11} - 10^{-10}$  m<sup>2</sup>. The apparent permeability shows significant fluctuations that correlate with the decompression rate,  $-dP_1/dt$ , as shown by Figure 5d (red curve). When the decompression rate increases, the apparent permeability also increases.

#### 4.2. Parameter Dependence of Outgassing

Figure 6 summarizes the observed outgassing characteristics. Outgassing must be related to the increased volume of gas inside the foam that is associated with decompression. Thus, we plotted Figures 6a–6c as a function of the volumetric foam expansion rate, which is calculated by the pressure change measured inside the foam [Namiki and Manga, 2006]

$$-\frac{\phi}{P_1} \frac{dP_1}{dt} \tag{8}$$

Equation (8) indicates the possible expansion of gas inside the foam under the constant temperature associated with externally imposed pressure change.

The outgassing velocity defined in equation (7) is the most fundamental measurement for evaluating outgassing. Dividing equation (7) by the foam height, we obtain

$$\frac{v_{or}}{l} = -\frac{\phi}{P_1} \frac{dP_1}{dt} - \frac{1}{V_{fm}} \frac{dV_{gm}}{dt} \tag{9}$$

In the right-hand side of equation (9), the first term is the expansion rate as defined in equation (8), and the second term indicates the measured expansion of the gas remaining inside the foam.

Figure 6a plots the outgassing rate,  $v_{or}/l$ , as a function of the expansion rate and shows that the outgassing rate basically becomes larger with the expansion rate. In Figure 6a, some symbols are located on the black line. On the black line with slope 1,  $v_{or}/l$  is consistent with the expansion rate, indicating that the foam does not expand; i.e., all of the increased volume of gas by decompression outgases. At this stage, there were no further expansions of the foam, irrespective of decompression. In most cases, smaller symbols are plotted on the black line and larger symbols are plotted beneath the black line. Here, the size of the symbol becomes smaller as more time elapsed. This result suggests that foams expand at an early stage of decompression, and outgassing becomes dominant with the passage of time. There are two possible explanations for this time evolution: (1) Bubbles expand to make films thinner, which enables the propagation of film ruptures and (2) with the resultant film ruptures, several pathways for outgassing are generated.

Figure 6b shows that the vertical pressure gradient increases with the expansion rate and the vertical pressure gradient is larger for more viscous liquids. This is because, for a rapid decompression with a viscous liquid, each bubble does not expand rapidly, so the pressure inside the foam remains at higher pressure than that outside the foam.

Apparent permeability,  $k$ , in equation (6) is a ratio of the outgassing velocity and the vertical pressure gradient; both have expansion rate dependence, with the result that apparent permeability does not show the expansion rate dependence, as shown in Figure 6c. Except for Run 7, denoted by plus, apparent permeability increases with the gas fraction, as shown in Figure 6d. This may be because, for larger  $\phi$ , the number of sufficiently thin films to initiate the propagation of film ruptures increases.

The apparent permeability of Run 7 varies in a wide range at an almost constant gas fraction,  $\phi \sim 0.6$ , suggesting an importance of hysteresis. In Run 7, we waited for 1 day after making the foam before starting the experiment in order to increase the bubble size. During this waiting time, a hard surface of syrup formed at the top of the foam by the evaporation of water. When the pathway generated by film ruptures in association with decompression, the pathway can remain in the same place longer. If pathways appear at the beginning of the decompression, in which the expansion rate is high and persists for a long time because of its high viscosity, the permeability also remains high even after the expansion rate becomes low. This hypothesis is consistent with the fact shown in Figure 6b. The vertical pressure gradient becomes low with elapsed time irrespective of high-viscosity and high-expansion rate, suggesting that the pathways continue to release gas inside the foam to reduce the overpressure. The large initial bubble sizes in Run 7 also can make the apparent permeability high. Permeability usually increases with the square of the bubble size. Given that highly permeable pathways exist in the foam, Run 7 shown by pluses overlaps with the black line in Figure 6a, in which the foam does not expand in association with decompression.

#### 4.2.1. Interpretation of Measured Apparent Permeability

The calculated apparent permeabilities for our experiments are less than  $< 10^{-9} \text{ m}^2$ . Using the Kozeny-Carman equation  $k = D^2/180 \cdot \phi^3/(1 - \phi)^2$  with assumptions of  $D = 10^{-4} \text{ m}$  and  $\phi = 0.9$ , the permeability is estimated as  $k > 10^{-9} \text{ m}^2$ . The apparent permeabilities measured in our experiments are lower than those estimated with the Kozeny-Carman equation with smaller bubble sizes than those in our experiments. Here, in the Kozeny-Carman equation, it is assumed that an interconnected structure exists stably. In contrast, the interconnected structure exists only occasionally in our experiments. The apparent permeability measured in our experiments suggests that the liquid film separating each bubble prevents outgassing.

On the other hand, the maximum apparent permeability in these experiments can exceed the measured permeability of natural samples ( $< 10^{-11} \text{ m}^2$ ). Here, the natural samples are solid magma so that the pathway for outgassing can exist stably. In contrast, our syrup is liquid, and the pathway for outgassing intermittently opens and closes. This is contrary to intuition, which would suggest that the permeability for natural samples with stable pathways would be higher than that for liquid foam with temporal pathways. We are aware of the large width of the pathway temporarily generated in the syrup foam, which can increase permeability because the permeability usually depends on the square of the pathway radius. Given that the temporal pathway closes after outgassing, we do not observe large pathways in the natural samples, and the measured permeability becomes lower. Thus, we conclude that should the propagation of film ruptures observed in our experiment occur in a real volcanic conduit, outgassing could become more efficient than has been previously estimated.

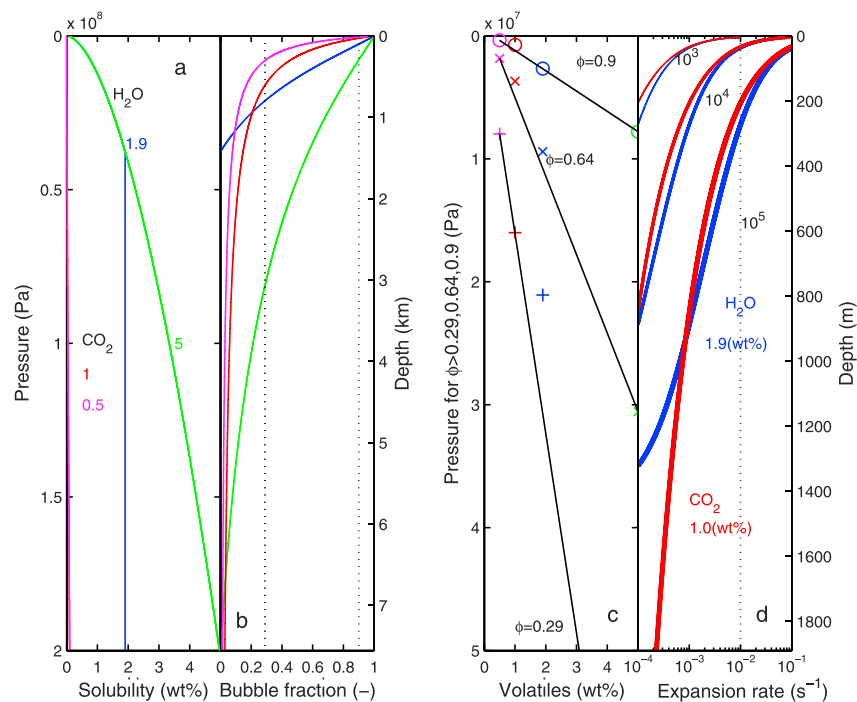


**Figure 7.** Estimates of conditions within a conduit, in which our experimental results are applicable. (a) Pressure-dependent solubility of water [Shishkina et al., 2010]. Colors indicate the initial volatile content in the melt; blue and green curves are for 1.9 and 5 wt % of H<sub>2</sub>O, and pink and red curves are for 0.5 and 1 wt % for CO<sub>2</sub>, respectively. We use the same colors for the curves in Figures 7b and 7c. (b) Volumetric gas fraction,  $\phi$ , as a function of pressure for the closed system. Dotted lines indicate  $\phi = 0.29$ , above which bubbles may start to be in contact with one another, and  $\phi = 0.9$ , the maximum gas fraction in our experiments. (c) The pressure ranges of  $\phi = 0.29, 0.64$ , and  $0.9$  as functions of the initial volatile fraction. (d) Expansion rates for magma with an initial volatile content of 1.9 wt % of H<sub>2</sub>O and 1 wt % of CO<sub>2</sub> as estimated by equation (8); colors indicate volatile species, and different curve widths show the decompression rates of  $10^3, 10^4$ , and  $10^5$  Pa s<sup>-1</sup>. Above the expansion rate of  $> 10^{-2}$  s<sup>-1</sup>, shown by a dotted line, we experimentally confirmed efficient outgassing (Figure 6a). In Figures 7a–7d, the right-hand axes indicate the scaled depths for bubble-free magma calculated by depth =  $P/\rho g$ . These are minimum estimates. In reality, the depth for a certain pressure that is estimated by depth =  $P/\rho(1 - \phi)g$  can become greater because of the existence of bubbles. Figures 7a–7b and 7c–7d share y axes, respectively.

## 5. Implications for Natural Systems

Our analogue experiments show that the propagation of film ruptures is faster than the ascent of large bubbles. The apparent permeabilities measured in our experiments are higher than those of natural pumices and scoriae. Thus, we infer that the upward propagation of film ruptures is an important mechanism for transporting volcanic gas rapidly to the atmosphere. Here we specify the possible conditions in a real volcanic conduit in which our experimental results are applicable.

In our experiments, outgassing by the propagation of film ruptures occurs efficiently when the gas fraction in the foam is high (Figure 6d). We experimentally confirmed that the outgassing associated with film ruptures occurs at  $\phi > 0.7$ , but we did not constrain the lower limit of  $\phi$  for film ruptures. We infer that the propagation of film ruptures occurs if the bubbles are in contact, making a thin film. There are roughly two models for describing this condition. One is the percolation threshold for randomly distributed bubbles, which is estimated to be  $\phi \sim 0.29$  by numerical simulation [Garboczi et al., 1995]. The other is random close packing of bubbles. Randomly distributed bubbles may be able to float and to be closely packed, where the bubble fraction is  $\phi \sim 0.64$  [e.g., Torquato et al., 2000; Song et al., 2008]. We next calculate the possible  $\phi$  distribution within a conduit.

To estimate the bubble distribution in a conduit, we use a solubility curve [e.g., Dixon, 1997; Newman and Lowenstern, 2002; Papale et al., 2006; Shishkina et al., 2010]. Figure 7a shows vertical profiles of dissolved volatile content in a conduit with several initial values calculated after Shishkina et al. [2010]. We plot 0.5 and 1 wt % for CO<sub>2</sub> and 1.9 and 4 wt % for H<sub>2</sub>O. These are typical values for volatile contents [Wallace, 2005]. The initial volatile content of magma from the 2000 eruption of Miyakejima Volcano is estimated as 1.6–1.9 wt % of H<sub>2</sub>O and 0.08–0.1 wt % of CO<sub>2</sub> [Saito et al., 2005].

The bubble fraction is determined by the amount of exsolved volatiles depending on the solubility and initial content of volatiles in the melts. We do not consider the relative velocity between bubbles and the surrounding melt, since this process is too complex to estimate the resulting profiles [e.g., *Vergnolle and Jaupart, 1990; Phillips and Woods, 2001*]. For simplicity, we assume here that the bubble fraction is determined by an exsolution solely of H<sub>2</sub>O or CO<sub>2</sub>. Assuming that all of the exsolved volatiles form bubbles without outgassing, we can calculate the bubble fraction as a function of the exsolved mass fraction of volatiles  $n$ ,

$$\phi = \frac{1}{\left(\frac{1}{n} - 1\right) \frac{\rho_g}{\rho} + 1}, \quad (10)$$

where  $\rho \sim 2700 \text{ kg m}^{-3}$  is the density of the melt and  $\rho_g$  is the density of H<sub>2</sub>O or CO<sub>2</sub> gas. Here, we calculate the density of the gas by  $\rho_g = P/(R_g T)$ , where  $R_g$  is the specific gas constant, and we assume the temperature of  $T = 1000^\circ\text{C}$ .

Figure 7b plots the calculated vertical profiles of the bubble fraction and shows that the bubble fraction becomes larger at a shallower depth. At a deeper part, because of its low solubility, more CO<sub>2</sub> bubbles exist than those of H<sub>2</sub>O. In contrast, at a shallower depth, more H<sub>2</sub>O bubbles exist because of the higher initial water content.

Figure 7c shows that the percolation threshold for randomly distributed bubbles,  $\phi > 0.29$ , appears at several 10 MPa that correspond to a depth of  $< 1 \text{ km}$  for magma with an initial water content of 2 wt %. The bubble fraction at random close-packing  $\phi > 0.64$  is achieved only in the low-pressure region of  $< 30 \text{ MPa}$ , even with a large initial water content of 5 wt %, which corresponds to a depth of 1 km for bubble-free magma. The bubble fraction  $\phi \sim 0.9$  is approximately the maximum observed in our experiments, in which the propagation of film ruptures occurs frequently. In Figure 7c, the region with a high bubble fraction  $\phi > 0.9$  is further limited at a very shallow depth ( $< 7 \text{ MPa}$ ).

In Figure 7d, we compare the possible expansion rate in a volcanic conduit with that of our experiments. Here we calculated the expansion rate by equation (8), using the bubble fraction obtained in Figure 7b. Our experiments were conducted in the range of expansion rate of  $> 10^2 \text{ s}^{-1}$  (Figure 6a), as shown by Figure 7d (dotted lines), in which outgassing associated with film ruptures was observed.

For a volcanic conduit, we calculate the expansion rate with decompression rates of  $10^3$ ,  $10^4$ , and  $10^5 \text{ Pa s}^{-1}$ , which approximately correspond to the ascent velocities of bubbly magma,  $4 \times 10^{-2}$ ,  $4 \times 10^{-1}$ , and  $4 \text{ m s}^{-1}$ , respectively. There is a pressure gradient in a volcanic conduit such that the expansion rate is determined by the ascent velocity of bubbly magma. This is different from our experiments, which are decompressed by a vacuum pump. We assume the initial volatile content of 1.9 wt % for H<sub>2</sub>O and 1 wt % for CO<sub>2</sub>. Figure 7d shows that, when magmas ascend rapidly, the propagation of film ruptures frequently occurs at a shallow region of  $< 5 \text{ MPa}$  to make the bubble fractions in magmas their maximum.

The occurrence of outgassing is sometimes discussed by comparing the magma ascent velocity with outgassing velocity. The observed outgassing velocity in our experiments are less than  $0.1 \text{ m s}^{-1}$  and can be lower than the assumed ascent velocity of magmas in Figure 7d. Here, we consider that the outgassing velocity should be a relative velocity to the magma ascent and outgassing can occur irrespective of the magma ascent velocity.

Geochemical observations have revealed that the segregation of volcanic gas from the surrounding magma occurs at a very shallow region without eruption, suggesting that magma that is losing bubbles becomes heavier and descends back to the depths, which is known as magma convection in a conduit [*Shinohara, 2008*]. However, the mechanism for segregating bubbles from the melt has been unknown. The upward propagation of film ruptures can segregate the gas inside bubbles from the surrounding melt to send the dense melt back to the depths, which becomes a driving force for maintaining convection in a conduit.

Another important aspect of our experiments is that the propagation of film rupturing causes intermittent outgassing from the pathway. Except for Run 7, our experiments show that the outlet of the pathway closes after an instance of outgassing. In addition, the fluctuation of pressure data is correlated with the change in foam volume in Figure 5c. These results suggest that the pathway made by the film rupturing closes in a relatively short time, so that outgassing becomes intermittent. This view is quite different from the continuous permeable gas flow that has been widely assumed. When the viscosity of magma is large enough, the

timescale until the outlet is closing may increase so that the outgassing could become more continuous, as observed in Run 7. If the pathway made by the propagation of film rupturing continues at a depth of several kilometers, such a pathway may be able to rapidly transport gas from the depths, causing an explosive gas emission [Burton *et al.*, 2007; Aiuppa *et al.*, 2010].

## 6. Conclusion

We conducted a series of slow decompression experiments using syrup foam as a magma analogue. The experiments showed the upward propagation of void expansions and intermittent outgassing. The upward propagation of void expansion velocity is regulated by the film-rupturing velocity, suggesting that the propagation of film ruptures originates outgassing. Outgassing by the propagation of film ruptures occurs efficiently when the bubble fraction is large,  $\phi > 0.7$ .

In a real volcanic conduit, the bubble fraction becomes high at the top of the magma column. It has been suggested that volcanic gas separates from the surrounding magma at the top of the magma column, which is known as the magma column convection model [Shinohara, 2008]. The propagation of film ruptures observed in our experiments appears to be the mechanism for separating volcanic gasses from the surrounding magma at the top of the magma column. The depleted magma in volatile components becomes heavier than the newly ascending magma and so descends to support convection within the conduit.

## Appendix A: Rupture of a Liquid Film Surrounding an Isolated Bubble

### A1. Film Rupture Velocity

Kobayashi *et al.* [2010] observed the growth of an aperture on an isolated bubble film made of aqueous syrup with various volumes of bubbles surrounded by various liquid viscosities. In order to understand film ruptures within a syrup foam shown in Figure 3, we reference the results of Kobayashi *et al.* [2010].

Figure A1 shows their original data: time-dependent aperture growth on a bubble film. The color indicates the difference in syrup viscosity. For larger liquid viscosities, apertures grow slowly.

The aperture growth first accelerates, then decelerates, and finally stops at a certain radius. In these experiments, the bubble deflates after the aperture growth halts, suggesting that when the gas inside the bubble escapes to the outside of the bubble through the aperture, the bubble film loses tensional force so that aperture growth stops. The deceleration of aperture growth does not represent the physics of film rupturing. Thus, we calculated slopes of the aperture growth as shown in Figure A1 until the aperture growth velocity was at its maximum and plotted it as the film rupture velocity in Figure 3a. In Figure 3a, each black bullet shows the averaged velocity among experiments with the same bubble volumes and same liquid viscosities. The error bar indicates the minimum and maximum velocity among experiments with the same liquid viscosities.

### A2. Thickness of a Bubble Film

In order to calculate the film rupture velocity, we need to know the bubble film thickness. In Figures 3a and 3b, we used the estimated bubble film thickness of Kobayashi *et al.* [2010]. Integrating equation (3), we obtained the aperture radius on a rupturing film as a function of time  $t$ ,

$$r(t) = r_0 \exp\left(\frac{\gamma}{\eta e} t\right). \quad (\text{A1})$$

By fitting the measured aperture growth as shown in Figure A1 with equation (A1) until each slope becomes maximum, we obtained the film thickness,  $e$ , and initial aperture radius,  $r_0$ , simultaneously, and plot the thickness in Figure 3b. Each black bullet indicates the averaged film thickness among experiments with the same liquid viscosity, and the error bar shows the minimum and maximum film thickness. Using four bullets  $\eta > 5 \text{ Pa s}$ , we obtain  $e = 3 \times 10^{-5} \eta^{-0.62}$ , plotted in Figure 3b (red line). For a less viscous liquid film, the rupture velocity follows equation (2), and its film thickness cannot be estimated by this method. We thus use experiments with large liquid viscosities.

Similarly, we obtained  $r_0 = 3 \times 10^{-4} \eta^{-0.03}$ , which is approximately constant of  $3 \times 10^{-4} \text{ m}$ . In Kobayashi *et al.* [2010], the value of  $r_0$  represents the time and space resolution of the high-speed camera rather than the physically determined initial size of the apertures.

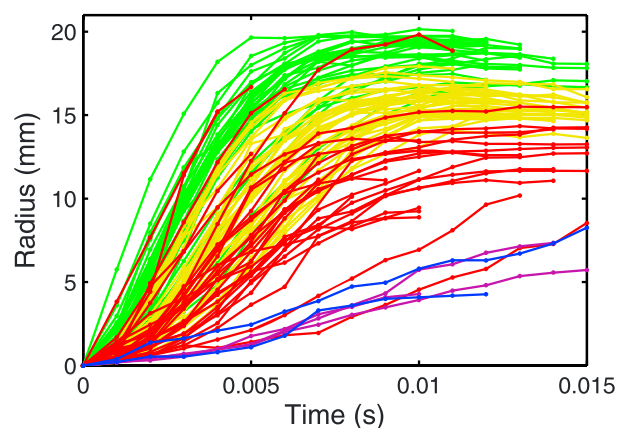


**Figure A1.** Time evolution of aperture radii on isolated bubbles. Colors of green, yellow, red, purple, and blue indicate differences in liquid viscosity, 1.9, 7.8, 37, 68, and 120, respectively. Modified from Kobayashi *et al.* [2010].

thickness surrounding apertures using the growth rate, with the result that their estimate becomes thicker than the critical thickness for rupturing. Here, Figure A1, shows that an aperture on a less viscous liquid film can grow larger. At a greater aperture radius, the film thickness must become thicker. We infer that the viscosity dependence of estimated film thickness shown in Figure 3b is originated from the difference of final aperture radius.

#### Acknowledgments

We thank Michael Manga for comments on an earlier version of our manuscript and Jess Robertson and an anonymous reviewer for their reviews. The high-intensity surface light source was provided by Sumita Optical Glass, Inc. Koso Syrup is provided by Japan Corn Starch Co., Ltd. This work is supported by KAKENHI 24681035.

#### References

- Aiuppa, A., A. Bertagnini, N. Metrich, R. Moretti, A. D. Muro, M. Liuzzo, and G. Tamburello (2010), A model of degassing for Stromboli Volcano, *Earth Planet. Sci. Lett.*, *295*, 195–204.
- Bagdassarov, N., A. Dorfman, and D. B. Dingwell (2000), Effect of alkalis, phosphorus, and water on the surface tension of haplogranite melt, *Am. Mineral.*, *85*, 33–40.
- Barmin, A., O. Melnik, and R. S. J. Sparks (2002), Periodic behavior in lava dome eruptions, *Earth Planet. Sci. Lett.*, *199*, 173–184.
- Bello, E. D., E. W. Llewellyn, J. Taddeucci, P. Scarlato, and S. J. Lane (2012), An analytical model for gas overpressure in slug-driven explosions: Insights into Strombolian volcanic eruptions, *J. Geophys. Res.*, *117*, B02206, doi:10.1029/2011JB008747.
- Brenner, M. P., and D. Gueyffier (1999), On the bursting of viscous films, *Phys. Fluids*, *11*, 737–739.
- Burgisser, A., and J. E. Gardner (2005), Experimental constraints on degassing and permeability in volcanic conduit flow, *Bull. Volcanol.*, *67*, 42–56.
- Burnett, G. D., J. J. Chae, and W. Y. Tam (1995), Structure and dynamics of breaking foams, *Phys. Rev. E*, *51*, 5788–5796.
- Burton, M., P. Allard, F. Mure, and A. L. Spina (2007), Magmatic gas composition reveals the source depth of slug-driven Strombolian explosive activity, *Science*, *2007*, 227–230.
- Castro, J. M., A. Burgisser, C. I. Schipper, and S. Mancini (2012), Mechanisms of bubble coalescence in silicic magmas, *Bull. Volcanol.*, *74*, 2339–2352.
- Colo, L., M. Ripepe, D. R. Baker, and M. Polacci (2010), Magma vesiculation and infrasonic activity at Stromboli open conduit volcano, *Earth Planet. Sci. Lett.*, *292*, 274–280.
- Culick, F. E. C. (1960), Comments on a ruptured soap film, *J. Appl. Phys.*, *31*, 1128–1129.
- Debrégeas, G., P. G. de Gennes, and F. Brochard-Wyart (1998), The life and death of “bare” viscous bubbles, *Science*, *279*, 1704–1707.
- Dixon, J. E. (1997), Degassing of alkalic basalts, *Am. Mineral.*, *82*, 368–378.
- Edmonds, M., T. M. Gerlach, and R. A. Herd (2009), Halogen degassing during ascent and eruption of water-poor basaltic magma, *Chem. Geol.*, *263*, 122–130.
- Eichelberger, J. C., C. R. Carrigan, H. R. Westrich, and R. H. Price (1986), Non-explosive silicic volcanism, *Nature*, *323*, 598–602.
- Garboczi, E. J., K. A. Snyder, and J. F. Douglas (1995), Geometrical percolation threshold of overlapping ellipsoids, *Phys. Rev. E*, *52*, 819–828.
- Gardner, J. E. (2012), Surface tension and bubble nucleation in phonolite magmas, *Geochim. Cosmochim. Acta*, *76*, 93–102.
- Giordano, D., and D. Dingwell (2003), Viscosity of hydrous Etna basalt: Implications for Plinian-style basaltic eruptions, *Bull. Volcanol.*, *65*, 8–14.
- Gonnermann, H. M., and M. Manga (2013), Dynamics of magma ascent in the volcanic conduit, in *Modeling Volcanic Processes*, edited by S. A. Fagents, T. K. P. Gregg, and R. M. C. Lopes, pp. 55–84, Cambridge Univ. Press, Cambridge, U. K.
- Hasmy, A., R. Paredes, O. Sonnevile-Aubrun, B. Cabane, and R. Botet (1999), Dynamical transition in a model for dry foams, *Phys. Rev. Lett.*, *82*, 3368–3371.
- Houghton, B. F., C. J. N. Wilson, P. D. Carlo, M. Coltelli, J. E. Sable, and R. Carey (2004), The influence of conduit processes on changes in style of basaltic Plinian eruptions: Tarawera 1886 and Etna 122 BC, *J. Volcanol. Geotherm. Res.*, *137*, 1–14.
- James, M. R., S. J. Lane, L. Wilson, and S. B. Corder (2009), Degassing at low magma-viscosity volcanoes: Quantifying the transition between passive bubble-burst and Strombolian eruption, *J. Volcanol. Geotherm. Res.*, *180*, 81–88.
- Klug, C., and K. V. Cashman (1996), Permeability development in vesiculating magmas: Implications for fragmentation, *Bull. Volcanol.*, *58*, 87–100.
- Kobayashi, T., A. Namiki, and I. Sumita (2010), Excitation of airwaves caused by bubble bursting in a cylindrical conduit: Experiments and a model, *J. Geophys. Res.*, *115*, B10201, doi:10.1029/2009JB006828.
- Lindfors, K. R. (1924), Surface tension of sugar factory products, *Ind. Eng. Chem.*, *16*, 813–816.

In Figure 3b, the estimated film thickness is larger than 1  $\mu\text{m}$  and becomes thinner for a more viscous liquid with a slope of  $-0.6$ . In contrast, Nguyen *et al.* [2013] compiles measured film thicknesses just prior to spontaneous ruptures and shows that those thicknesses are on the order of 0.1–1  $\mu\text{m}$  without viscosity dependence, as shown by Figure 3b (blue-dotted rectangle). This discrepancy may arise from the nonuniform thicknesses of the bubble films. An aperture on a film appears at the thinnest region of the film as an initiation of a spontaneous rupture, while the growth rate of an aperture depends on the film thickness surrounding the aperture.

Kobayashi *et al.* [2010] estimate the film

- Mangan, M., and T. Sisson (2005), Evolution of melt-vapor surface tension in silicic volcanic systems: Experiments with hydrous melts, *J. Geophys. Res.*, *110*, B01202, doi:10.1029/2004JB003215.
- McKinley, G. H., and M. Renardy (2011), Wolfgang von Ohnesorge, *Phys. Fluids*, *23*, 127,101.
- Moitra, P., H. M. Gonnermann, B. F. Houghton, and T. Giachetti (2013), Relating vesicle shapes in pyroclasts to eruption styles, *Bull. Volcanol.*, *75*(691), 1–14.
- Mueller, S., B. Scheu, O. Spieler, and D. B. Dingwell (2008), Permeability control on magma fragmentation, *Geology*, *36*, 399–402.
- Namiki, A. (2012), An empirical scaling of shear-induced outgassing during magma ascent: Intermittent magma ascent causes effective outgassing, *Earth Planet. Sci. Lett.*, *353*, 72–81.
- Namiki, A., and M. Manga (2006), Influence of decompression rate on the expansion velocity and expansion style of bubbly fluids, *J. Geophys. Res.*, *111*, B11208, doi:10.1029/2005JB004132.
- Namiki, A., and M. Manga (2008), Transition between fragmentation and permeable outgassing of low viscosity magmas, *J. Volcano. Geotherm. Res.*, *169*, 48–60.
- Newman, S., and J. B. Lowenstern (2002), Volatilecalc: A silicate melt-H<sub>2</sub>O-CO<sub>2</sub> solution model written in Visual Basic for excel, *Comput. Geosci.*, *28*, 597–604.
- Nguyen, C. T., H. M. Gonnermann, Y. Chen, C. Huber, A. A. Maiorano, A. Gouldstone, and J. Dufek (2013), Film drainage and the lifetime of bubbles, *Geochem. Geophys. Geosyst.*, *14*, 3616–3631, doi:10.1002/ggge.20198.
- Okumura, S., M. Nakamura, S. Takeuchi, A. Tsuchiyama, T. Nakano, and K. Uesugi (2009), Magma deformation may induce non-explosive volcanism via degassing through bubble networks, *Earth Planet. Sci. Lett.*, *281*, 267–274.
- Okumura, S., M. Nakamura, T. Nakano, K. Uesugi, and A. Tsuchiyama (2012), Experimental constraints on permeable gas transport in crystalline silicic magmas, *Contrib. Mineral. Petrol.*, *164*, 493–504.
- Oldenziel, G., R. Delfos, and J. Westerweel (2012), Measurements of liquid film thickness for a droplet at a two-fluid interface, *Phys. Fluids*, *0022106*.
- Palma, J. L., S. Blake, and E. S. Calder (2011), Constraints on the rates of degassing and convection in basaltic open-vent volcanoes, *Geochem. Geophys. Geosyst.*, *12*, Q11006, doi:10.1029/2011GC003715.
- Papale, P., R. Moretti, and D. Barbato (2006), The compositional dependence of the saturation surface of H<sub>2</sub>O+CO<sub>2</sub> fluids in silicate melts, *Chem. Geol.*, *229*, 78–95.
- Parfitt, E. A., and L. Wilson (2008), *Fundamentals of Physical Volcanology*, 230 pp., Blackwell publishing, Oxford.
- Phillips, J. C., and A. W. Woods (2001), Bubble plumes generated during recharge of basaltic magma reservoirs, *Earth Planet. Sci. Lett.*, *186*, 297–309.
- Pioli, L., C. Bonadonna, B. J. Azzopardi, J. C. Phillips, and M. Ripepe (2012), Experimental constraints on the outgassing dynamics of basaltic magmas, *J. Geophys. Res.*, *117*, B03204, doi:10.1029/2011JB008392.
- Polacci, M., D. R. Baker, L. Mancini, S. Favretto, and R. J. Hill (2009), Vesiculation in magmas from Stromboli and implications for normal Strombolian activity and paroxysmal explosions in basaltic systems, *J. Geophys. Res.*, *114*, B01206, doi:10.1029/2008JB005672.
- Ripepe, M., A. J. L. Harris, and R. Carniel (2002), Thermal, seismic and infrasonic evidences of variable degassing rates at Stromboli Volcano, *J. Volcanol. Geotherm. Res.*, *118*, 285–297.
- Rust, A. C., and K. V. Cashman (2004), Permeability of vesicular silicic magma: Inertial and hysteresis effects, *Earth Planet. Sci. Lett.*, *228*, 93–107.
- Rust, A. C., and K. V. Cashman (2011), Permeability controls on expansion and size distributions of pyroclasts, *J. Geophys. Res.*, *116*, B11202, doi:10.1029/2011JB008494.
- Saito, G., K. Uto, K. Kazahaya, H. Shinohara, Y. Kawanabe, and H. Satoh (2005), Petrological characteristics and volatile content of magma from the 2000 eruption of Miyakejima Volcano, Japan, *Bull. Volcanol.*, *67*, 268–280.
- Sato, M., and I. Sumita (2007), Experiments on gravitational phase separation of binary immiscible fluids, *J. Fluid Mech.*, *591*, 289–319.
- Seyfried, R., and A. Freundt (2000), Experiments on conduit flow and eruption behavior of basaltic volcanic eruptions, *J. Geophys. Res.*, *105*, 23,727–23,740.
- Shinohara, H. (2008), Excess degassing from volcanoes and its role on eruptive and intrusive activity, *Rev. Geophys.*, *46*, RG4005, doi:10.1029/2007RG000244.
- Shishkina, T. A., R. E. Botcharnikov, F. Holtz, R. R. Almeev, and M. V. Portnyagin (2010), Solubility of H<sub>2</sub>O- and CO<sub>2</sub>-bearing fluids in tholeiitic basalts at pressures up to 500 MPa, *Chem. Geol.*, *277*, 115–125.
- Song, C., P. Wang, and H. A. Makse (2008), A phase diagram for jammed matter, *Nature*, *453*, 629–632.
- Spiegel, O., B. Kennedy, U. Kueppers, D. B. Dingwell, B. Scheu, and J. Taddeucci (2004), The fragmentation threshold of pyroclastic rocks, *Earth Planet. Sci. Lett.*, *226*, 139–148.
- Takeuchi, S. (2011), Preeruptive magma viscosity: An important measure of magma eruptibility, *J. Geophys. Res.*, *116*, B10201, doi:10.1029/2011JB008243.
- Takeuchi, S., A. Tomiya, and H. Shinohara (2009), Degassing conditions for permeable silicic magmas: Implications from decompression experiments with constant rates, *Earth Planet. Sci. Lett.*, *283*, 101–110.
- Torquato, S., T. M. Truskett, and P. G. Debenedetti (2000), Is random close packing of spheres well defined?, *Phys. Rev. Lett.*, *84*, 2064–2067.
- Vergnolle, S., and G. Brandeis (1996), Strombolian explosions 1. A large bubble breaking at the surface of a lava column as a source of sound, *J. Geophys. Res.*, *101*, 20,433–20,447.
- Vergnolle, S., and C. Jaupart (1990), Dynamics of degassing at Kilauea Volcano, Hawaii, *J. Geophys. Res.*, *95*, 2793–2809.
- Wallace, P. (2005), Volatiles in subduction zone magmas: Concentrations and fluxes based on melt inclusion and volcanic gas data, *J. Volcanol. Geotherm. Res.*, *140*, 217–240.